Necessity for Using Nonlinear Structural Analysis in Designing Blades

Kyle K. Wetzel[1]
Wetzel Engineering, Inc.
Lawrence, Kansas USA

Abstract

An engineering analysis is presented for a certified commercial blade that has experienced operational failures. Most of the failures result from a single root cause, namely localized panel buckling. Analyses following the methods prescribed by the IEC 61400-1 standards and Germanischer Lloyd's guidelines for certification suggested the design was sound. These analyses employed linear methods using popular finite shell elements with linear displacement formulations and limited capabilities for modeling large strain, large rotation, or the influence of transverse strain. Additional finite element models were built with alternative finite elements with a quadratic displacement formulation and more sophisticated formulations for large strain and rotation and transverse strain. Linear buckling analyses with these models properly predicts premature failure at the location where blades have failed in the field at load factors well below 100% Design Load. Moreover, nonlinear, large displacement analysis has further shown bothersome divergent displacement behavior at even lower load factors. This analysis confirms that safety factors and extra margins associated with linear analysis methods prescribed by GL are in some cases nonconservative. The blade in question exhibits poor surface geometry that creates stress concentrations that are not fully captured by linear analysis. The author recommends that nonlinear analyses be required as part of the design evaluation for Type Certification of wind turbine rotor blades.

1. Background, Objectives, and Scope of Work

A commercial manufacturer of 2-MW class wind turbines has experienced repeated failures of 42-44m class blades following relatively short periods of operation.[2] Most of the blades in question have failed at essentially the same location in similar manners. Cracks occur in the glass face sheets of the sandwich core structure forward of the spar cap (i.e., girder) at a spanwise location approximately halfway between the root of the blade and the location of maximum chord length (i.e., in the so-called transition region). The author has conducted structural analyses of the said blade on behalf of the manufacturer to help identify the root cause of these cracks and potential solutions. In the course of this work, the author determined that various common techniques for structurally analyzing blades prove inadequate.

The Objective of the present paper is to identify shortcomings in common structural analysis techniques that fail to predict structural defects and to recommend preferred practices. The purposes of the present paper do not include an exhaustive examination of the particulars of the design of the blade in question or all of the details of the blade failures. For commercial reasons, the author is limited in presenting such information. However, such limitations do not impair the discussion of the differing results that have been obtained using different analysis techniques.

The Scope of Work as it pertains to the present paper includes

- building a finite element model of the blade
- performing structural analyses to identify the minimum loads at which failure can be expected,
- identifying shortcomings in particular approaches to analyses that may not adequately identify structural problems.

---

[1] *kkwetzel@yahoo.com*. 785-331-5321.

[2] *Considerations of confidentiality do not permit the author to identify the manufacturer or specifics of the turbine or blade that would enable identification of the manufacturer.*

2. Methods of Analysis

2.1. Finite Element Model

The author built a finite element model of the blade in the ANSYS commercial FEA package.[1] The first model used for the initial studies is shown in Figure 1. The inboard 16m of the blade surface and shear web were modeled using 17,500 8-node shell elements (SHELL99 or SHELL91), with a total of 52,500 nodes. These two elements are very commonly used to model thin composites due to the ease of modeling layered structures. The mesh density was increased in the vicinity of the cracks to approximately 50x50mm elements (25mm spacing between corner and mid-side nodes), as seen in the insert in Figure 1.

A second model of the blade was subsequently built using 65,000 SHELL181 4-node shell elements. This is a higher-order element with large strain capability and an element formulation that more fully captures the influence of the soft foam core material. The mesh of the sandwich panel between the girder and the leading edge from 3.8 to 7.8m from the blade root was refined so that in the vicinity of the crack the elements are approximately 25mm square (Figure 2). The nodal density is similar in the two models.

All details of the laminate schedule and blade structure were captured to the extent that they can be accurately modeled using shell elements. The laminate was modeled layer-by-layer through the layered material feature of the SHELL91, SHELL99, and SHELL181 elements. The material stiffness and strength properties used in the present report are summarized in Table 1. The properties were provided by the manufacturer and are based on materials testing.

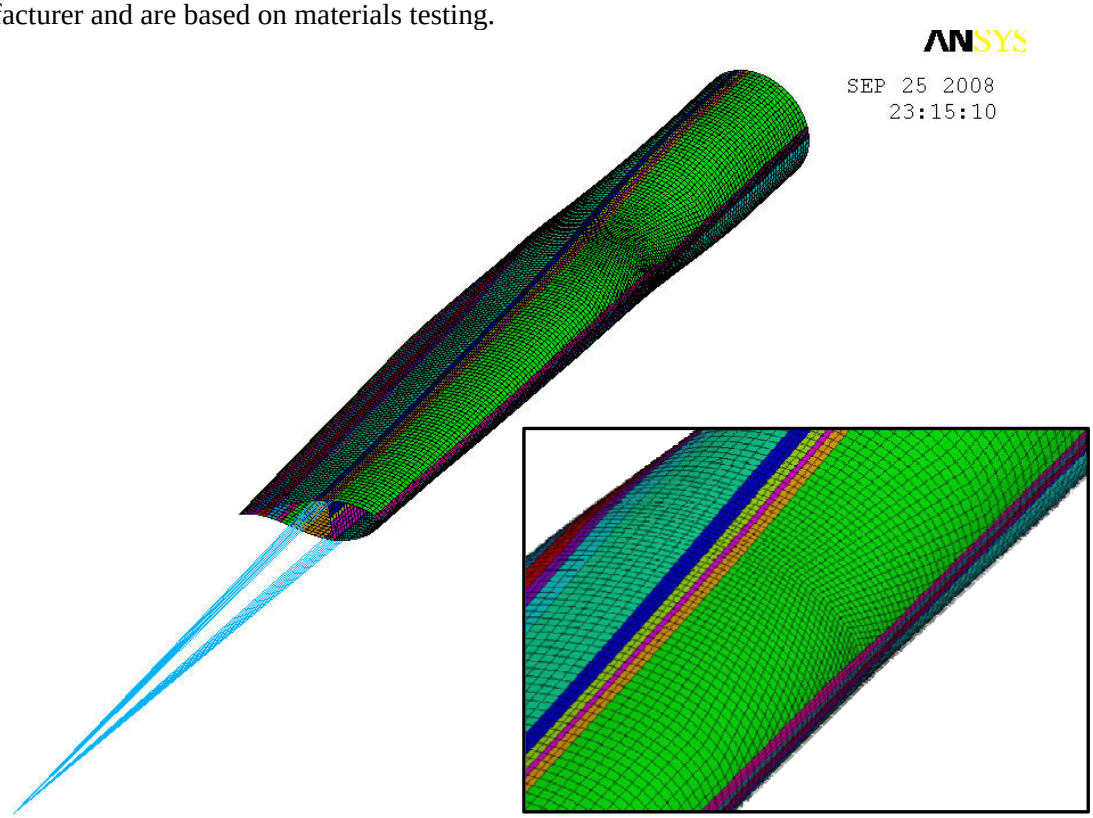

Figure 1. Finite Element Model 1

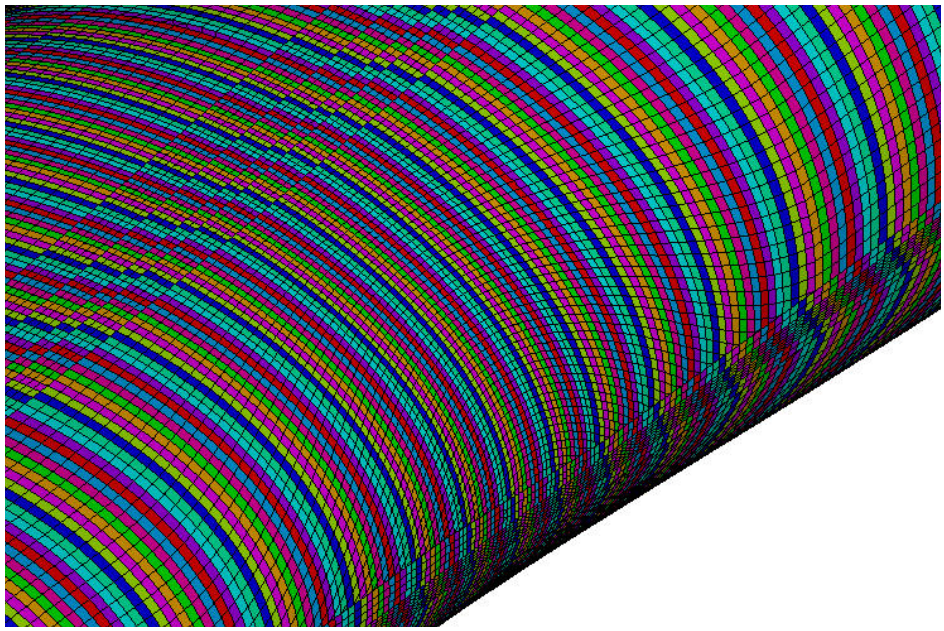

Figure 2. Closeup of Finite Element Mesh in Model 2 Near the Location of Cracks

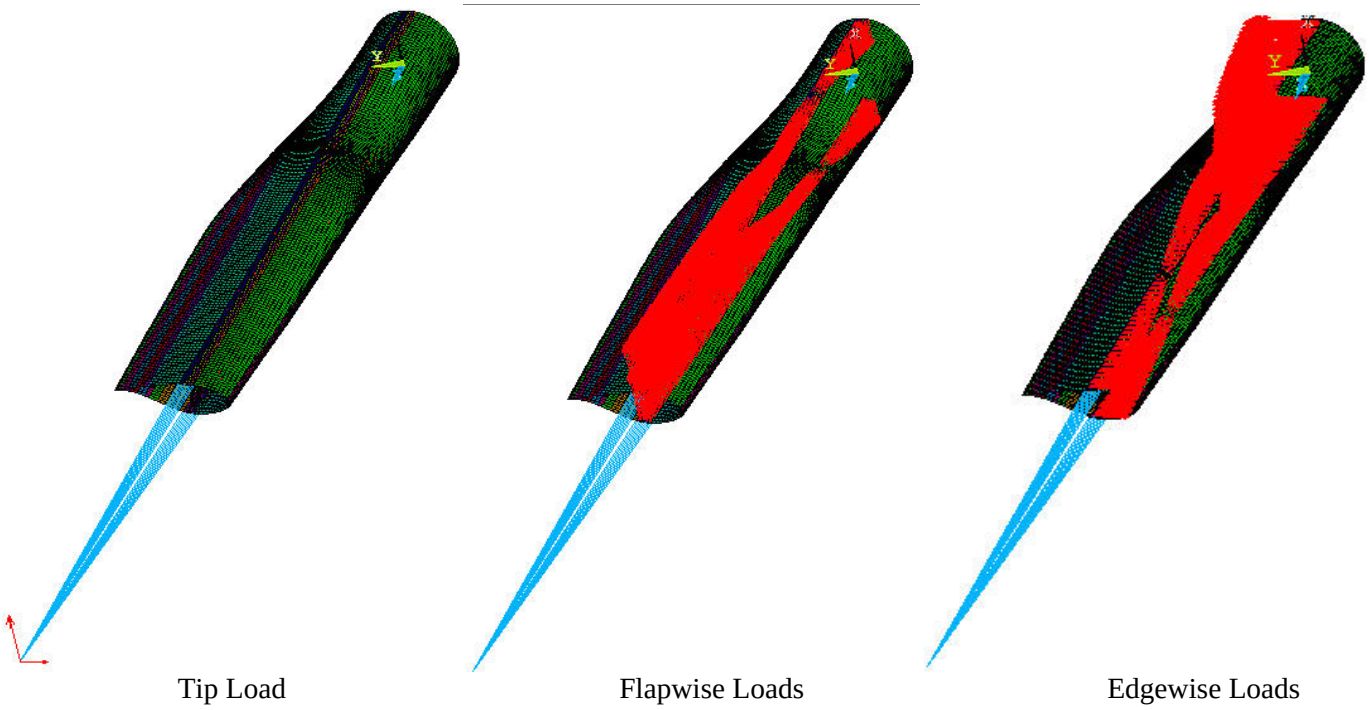

Figure 3. Loads Application to the Finite Element Model

The principal differences between the SHELL91 and 99 elements and the SHELL181 element are the formulation of rotational degrees of freedom and the influence of transverse (i.e., out-of-plane) characteristics on the stiffness matrix formulation. The SHELL181 element uses a penalty method to relate the independent rotational degrees of freedom about the normal (to the shell surface) with the in-plane components of displacements. This has a tendency to increase the energy content associated with rotational DOFs and can, therefore, influence the eigenvalues obtained from linear stability analyses.

More importantly, the SHELL181 elements also include a more accurate model of transverse shear deformation. An assumed shear strain formulation of Bathe-Dvorkin is used to alleviate shear locking. SHELL91 and 99 elements do not have this formulation and are subject to problems with shear locking. The calculation of transverse shear in these elements is approximate only and does not figure in to the energy of the element during solution. The transverse shear is calculated for the element as a whole, using a weighted average transverse shear modulus, G_{13} or G_{23}, for the element laminate. In this manner, it does not reflect the particular influence of any one layer, most importantly, the influence of the softer sandwich core. The SHELL181 formulation is performed layer-by-layer and is dependent on the transverse shear moduli of the materials of each layer. Therefore, the SHELL181 element more accurately captures the influence of core in sandwich construction. The significance of this is discussed further below in the results section.

The maximum loads determined from dynamic simulations of the turbine, plus safety factors as required by the IEC 61400-1 standard, and which were used for design purposes, were applied to the FEM. Loads were applied as a continuous distribution from root to tip, applied to the element corner nodes on the girder elements (Figure 3). The tip load was applied with a pilot node near Station 27000 and flexible BEAM4 elements attached to the girder nodes at Station 15000. The total stiffness of the beam elements matched the stiffness of the blade structure where they joined. This approach allowed a reduced model size, enabling a fine mesh model of the blade in the area of interest that could be solved relatively quickly for the nonlinear solutions. The nodes at the root of the blade were fixed against displacement with respect to all 6 degrees of freedom at each node.

Table 1. Material Properties used in the Present Analysis

	E11 [Pa]	E22 [Pa]	E33 [Pa]	G23 [Pa]	G13 [Pa]	G12 [Pa]	rho [kg/m^3]
Glass UD Girders, 53% fvf	3.690E+10	9.940E+09	9.940E+09	3.557E+09	3.557E+09	3.845E+09	1.857E+03
Glass UD TE, 51% fvf	3.690E+10	9.940E+09	9.940E+09	3.557E+09	3.557E+09	3.845E+09	1.857E+03
Glass UD other, 51% fvf	3.690E+10	9.940E+09	9.940E+09	3.557E+09	3.557E+09	3.845E+09	1.857E+03
Glass Triax, 51% fvf	2.429E+10	1.236E+10	9.940E+09	3.557E+09	3.557E+09	7.260E+09	1.826E+03
Glass DB, 51% fvf	1.170E+10	1.170E+10	9.943E+09	3.557E+09	3.557E+09	9.770E+09	1.889E+03
PVC Foam	4.50E+07	6.90E+07	6.90E+07	2.20E+07	2.20E+07	2.20E+07	6.00E+01
PS Foam	2.60E+07	2.60E+07	2.60E+07	6.20E+06	6.20E+06	6.20E+06	4.50E+01

	Axial Tension R11+ [Pa]	Axial Compression R11- [Pa]	Lateral Tension R22+ [Pa]	Lateral Compression R22- [Pa]	In-Plane Shear R12 [Pa]
Glass UD Girders, 53% fvf	6.820E+08	6.411E+08	3.500E+07	1.460E+08	5.700E+07
Glass UD TE, 51% fvf	6.820E+08	6.411E+08	3.500E+07	1.460E+08	5.700E+07
Glass UD other, 51% fvf	6.820E+08	6.411E+08	3.500E+07	1.460E+08	5.700E+07
Glass Triax, 51% fvf	4.360E+08	4.360E+08	8.000E+07	1.820E+08	1.200E+08
Glass DB, 51% fvf	1.800E+08	1.800E+08	1.800E+08	1.800E+08	2.000E+08

2.2. Results

2.2.1. SHELL91 and SHELL99 models

The Design Loads were applied to the model using SHELL99 elements, and a linear, small displacement static analysis was performed. The stress results in Layer 1 (the outer triaxial skin) were used to calculate the Puck exertion factors. The results are shown in Figure 4. The maximum predicted value is 1.012. Values are required to be less than 1.0. This means that the blade has a negative margin of safety of approximately 1.2%. The concentration occurs approximately 6m from the root of the blade. The stress concentration is approximately twice that of the region around the kink. It should be noted in passing that the original certification analysis showed a positive margin of safety. The reason for the small discrepancy observed in the present analysis is not known.

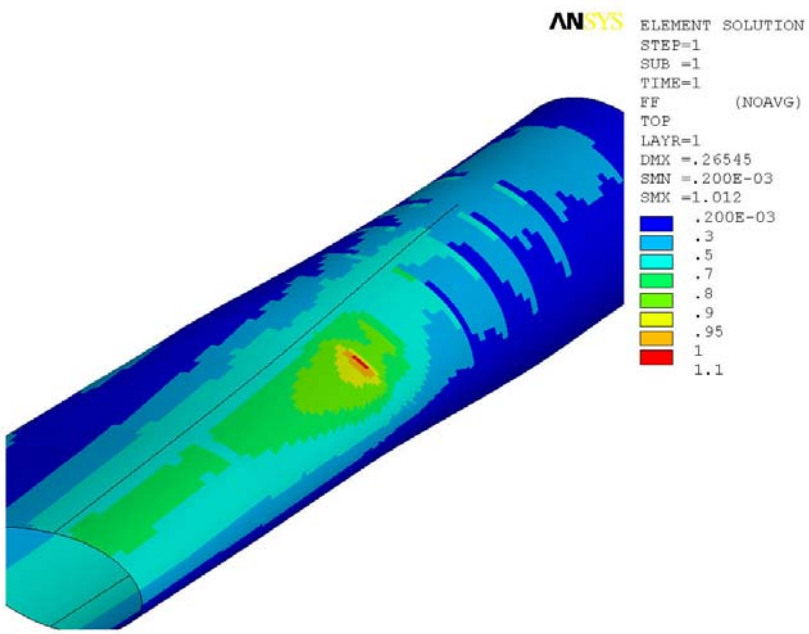

Figure 4. Outer Skin Puck Exertion Factor for Fiber Failure, Linear Solution

Design Load, Max Puck Exertion Factor = 1.012

The stress concentration is due in large part to a relatively severe concentration of concave curvature in the surface of the shell. Analysis of the geometry of the blade, as summarized in Figure 5 and Figure 6, shows significant flat spots forward of the girder. Figure 7 summarizes the resulting surface curvature on the nominally downwind side (where the cracks occur), which shows a significant spike approximately 6m from the blade root on all spanwise cross sections, but particularly between 700-800mm forward of the leading edge, where the curvature spikes at nearly 80mm/m^2. High concave curvature promotes buckling. One is essentially creating a crimp in the blade that will have reduced resistance to buckling. Obviously, a crimp will continue crimping further under load.

A linear (eigen) buckling analysis was conducted, which predicted buckling at a minimum load factor of 1.47, as shown in Figure 8. Germanischer Lloyd requires a minimum LF of 1.25 for linear analyses, and so the analysis would suggest that the present design is adequate.[2]

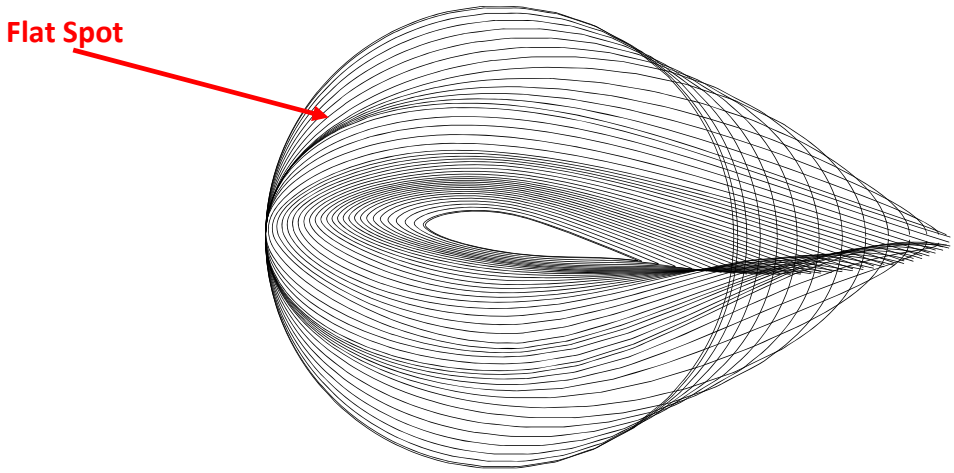

Figure 5. End View of Chordwise Cross Sections Through the Blade

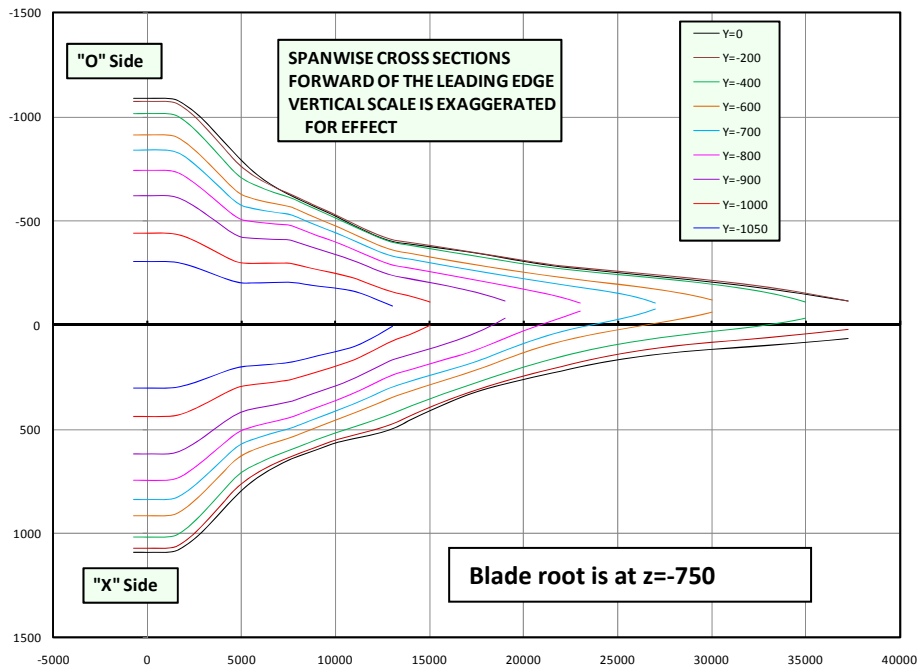

Figure 6. Spanwise Cross Sections Through the Leading Edge

The model was subjected to a large displacement (nonlinear geometry) static analysis. The linear geometric analysis of the previous section assumes that the geometric response everywhere is always proportional to the applied load. In a nonlinear, large displacement analysis, the applied load is increased in small steps. The displacement at any step is a function not only of the loads, but of the displacement itself. The solution is very localized. It is not assumed that the displacement at every point on the structure varies linearly with the load or proportionately with each other. For example, if a small region on the structure begins to buckle, then the displacement at that region will begin to diverge relative to the global displacement, or the displacement of points around the buckled region. By tracking the displacement at several points around a region, you can watch to see points near each other move in opposite directions as you increase the load. This is the sign that buckling is occurring.

Evidence of nonlinear divergence of the blade behavior is observed in Figure 9, which plots rotations of nodes in the vicinity of the cracks as load is increased. In the absence of local panel buckling, all of the nodes in one area should be rotating similarly as the load is increased. One would expect a slight increase in rotation moving outboard due to the larger deflection. The behavior exhibited in the figure is clearly evidence that nodes near each other are moving locally in different directions. This is evidence of the surface wave pattern produced by the local buckling. Note that in the vicinity of the crack (z=5000), nonlinear load-displacement response is observed almost from the outset of load application. This would suggest that the response is nonlinear at all loads. The presence of the kink essentially destabilizes the blade to the extent that nonlinear displacement behavior begins as soon as the load begins increasing.

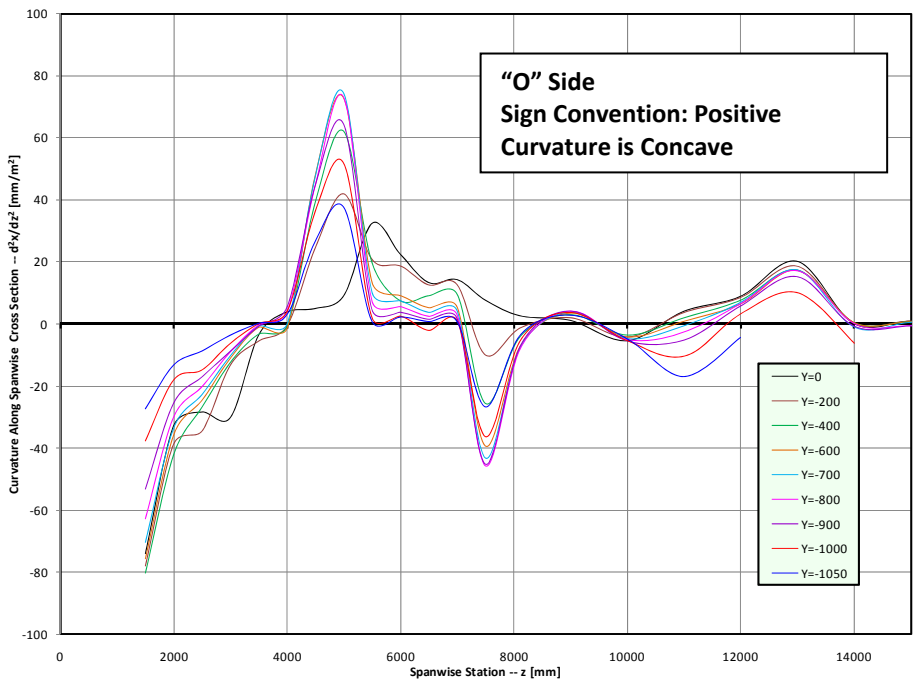

Figure 7. Curvature Along Spanwise Cross Sections Forward of the Girder

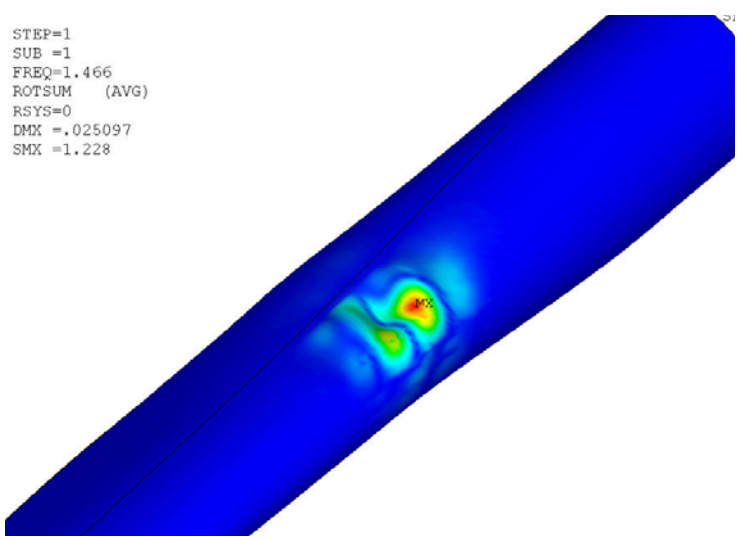

Figure 8. First Linear Buckling Mode, LF=1.47

At a load factor of only 20%, significant divergence is evidenced, and the model would not converge past 25% load, suggesting buckling had occurred. This is well below the linear prediction of 147%. Figure 10 illustrates the nonlinear buckling of the kinked region of the surface under load. This figure is taken from the solution at 25% Load. The scale of displacement is exaggerated 10-fold for clarity.

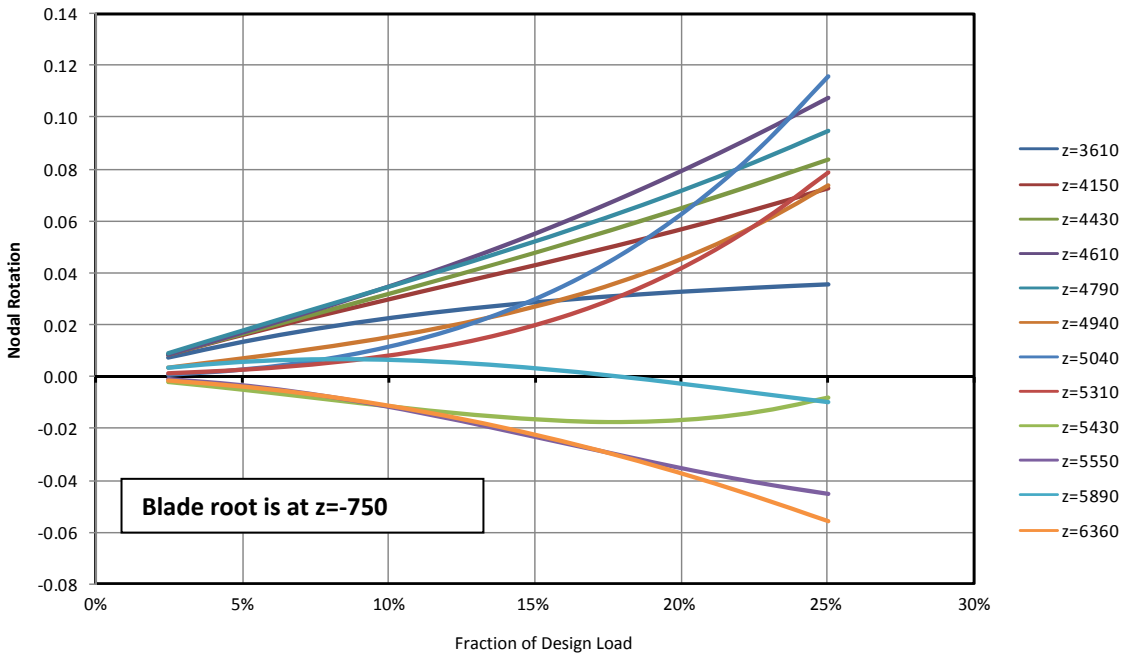

Figure 9. Nodal Rotations in the Vicinity of the Buckling

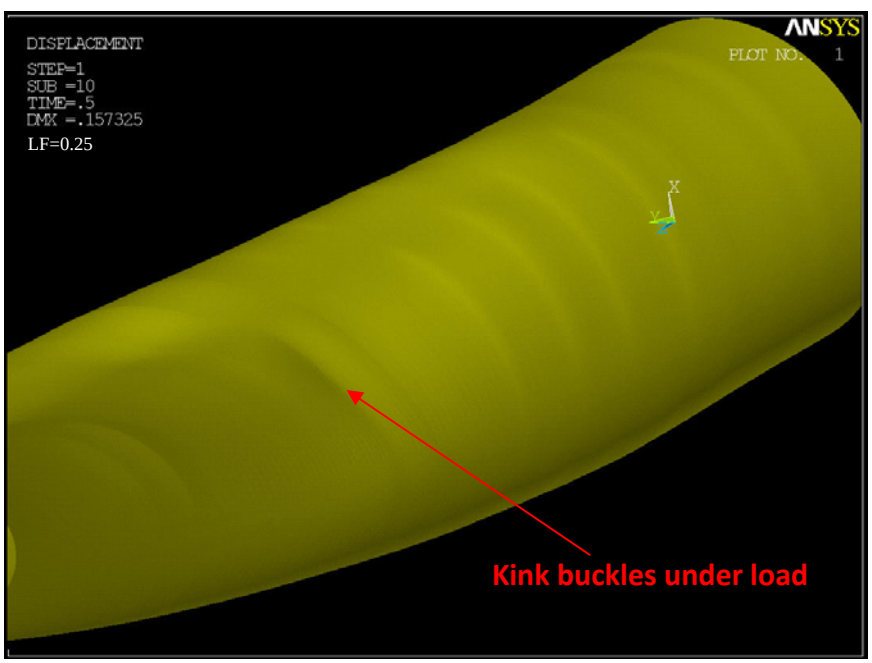

Figure 10. Nonlinear Buckling of the "O" Side (Scale Exaggerated)

2.3. SHELL181 model

With the SHELL181 model, linear and nonlinear buckling analyses predict buckling at the same load factor. The linear buckling analysis predicts buckling at a load factor of 27.1% of design load. The first buckling mode is shown in Figure 11(a). As the load is increased from 27.1% to 28.5% load, the buckled region expands both inboard and outboard. The buckling at 28.5% is shown in Figure 11(b). The pattern continues to progress like this, but it proved prohibitively time-consuming to try to extract more buckling modes from the program.

A large displacement static analysis was conducted to identify the stress concentrations near buckling. This was performed in load steps of 2.5% of the Design Load until 25% was reached, and was then continued in 1% increments to 27% of Design Load. The program could not converge at loads larger than 27% because of the first buckling mode shown in Figure 11. Figure 12 shows the buckling pattern just before the linear buckling load is reached.

Despite the much better agreement between the linear and nonlinear results, however, attention is drawn to the nodal rotations shown in Figure 13. Again, near the vicinity of buckling, nonlinear divergence actually begins at load factors as low at 10%, well below the 27% at which final buckling is predicted. While the SHELL181 element may be much more accurate in its linear buckling prediction, the linear buckling in and of itself is an inadequate method of predicting divergent behavior in structures with geometry defects.

3. Conclusions, Discussion and Recommendations

The results of the present study suggest that:

a) the results of linear buckling analyses can be highly sensitive to the particular element formulation employed. More specifically, higher-order elements such as the SHELL181 in ANSYS yield much more accurate linear buckling predictions than do elements with simpler formulations such as SHELL91 or SHELL99. The latter two are widely used, however, because of their ease of use.
b) even when using higher-order elements, however, linear buckling analyses, while accurately predicting final buckling, do not provide insight into nonlinearly divergent behavior that is occurring at load levels well below the minimum buckling load factor.
c) only nonlinear large-displacement analyses sufficiently capture divergent behavior. It is particularly important to employ such analyses to help identify local panel buckling due to poor blade surface geometry.

The degree to which the linear buckling analysis conducted with the finite element model using the SHELL91 and 99 elements failed to predict buckling is well outside of the margins of safety provided for by GL's guidelines. This analysis predicted failure at 147% of design load (versus minimum 125% in GL's guidelines), whereas failure is predicted at no more than 25% of design load using the nonlinear analysis with the same element and 27% using the SHELL181 element.

It is not known what the actual loads are in the field that produced the failures that have been observed, as the turbines experiencing such failure are not instrumented. However, a turbine that was instrumented for loads measurements exhibited peak loads in excess of 27% of design load, but well less than 100% of design loads. While this cannot serve as verification of the accuracy of the nonlinear buckling analyses, it can serve to document the fact that the more thorough analyses would have predicted blade failure at loads less than have been observed in the field.

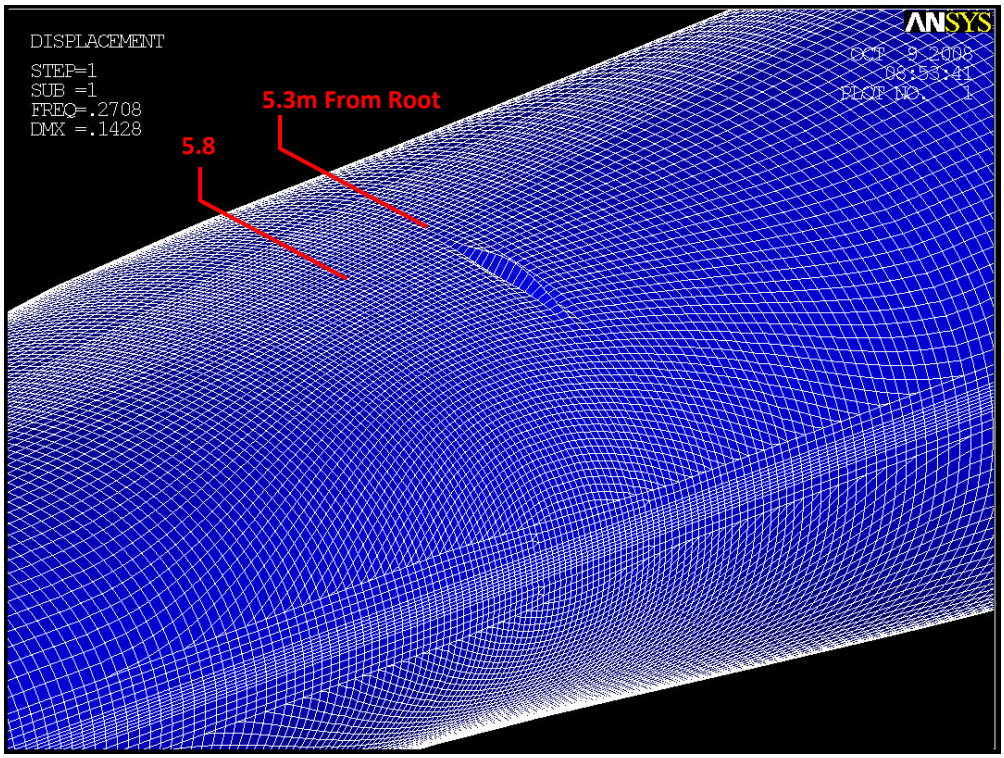

(a) First Buckling Mode, 27.1% of Design Load

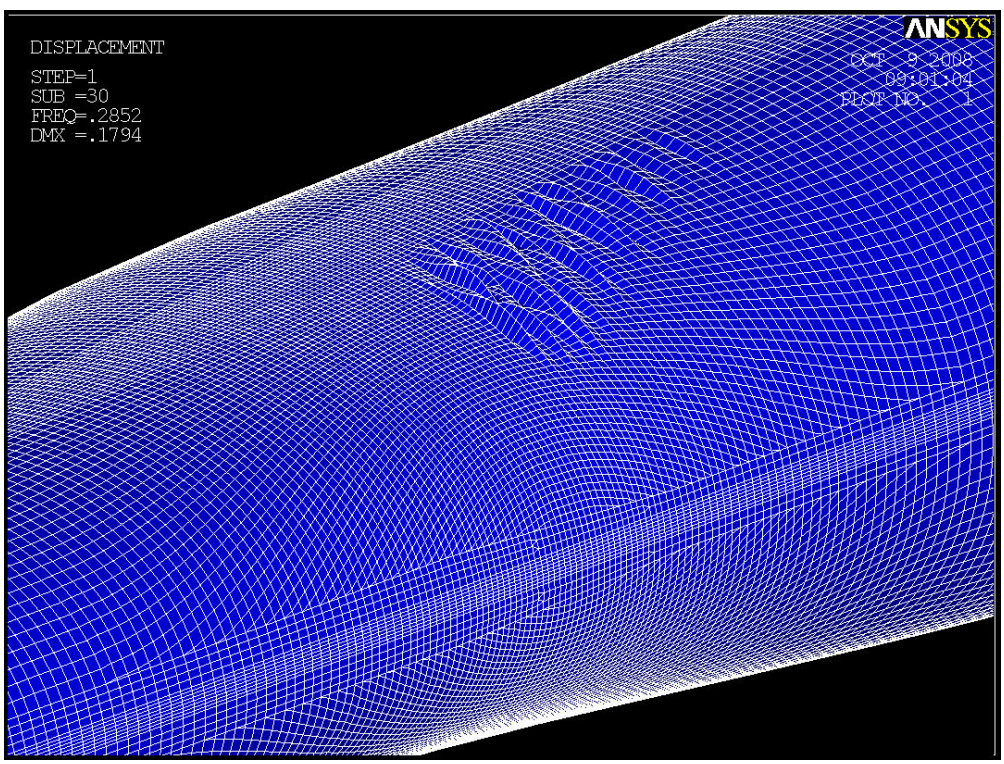

(b) Buckling Mode at 28.5% of Design Load

Figure 11. Linear Buckling of the "O" Side

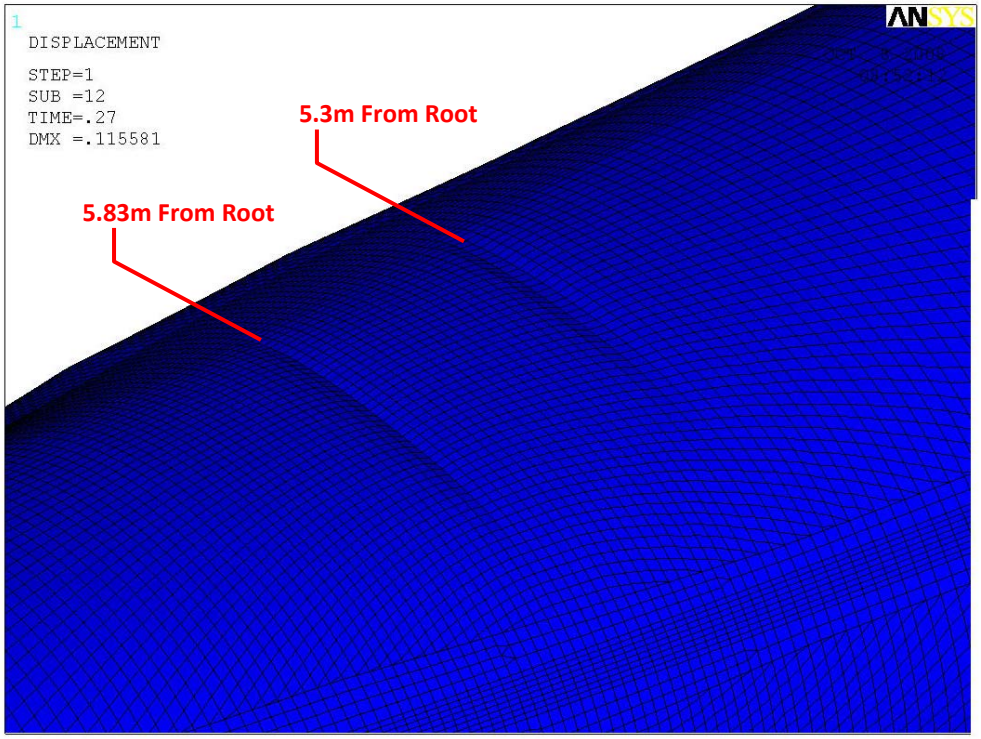

Figure 12. Nonlinear Buckling of the "O" Side (Scale Exaggerated)

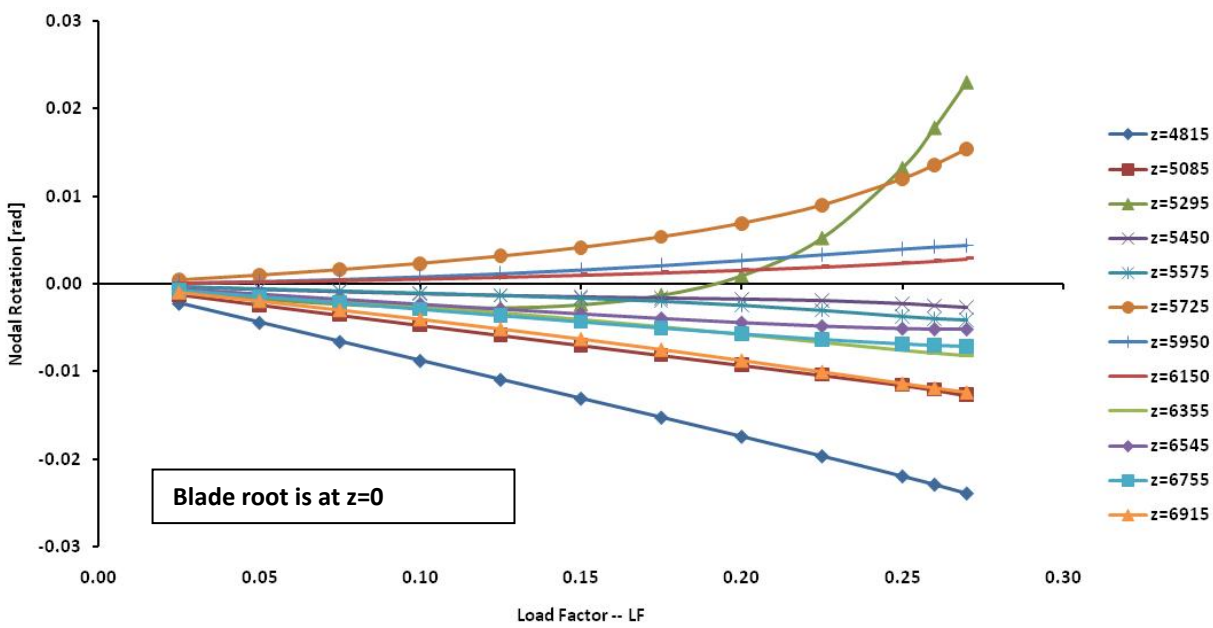

Figure 13. Nodal Rotations in the Vicinity of the Buckling

The exact reason for the superior agreement between the linear and nonlinear buckling analyses in the SHELL181 model versus the SHELL99 model can probably not be known, given the number of differences between the two elements. From discussions with ANSYS technical personnel, however, the author has concluded that the superior transverse shear formulation of the SHELL181 element is the most likely reason. Transverse strain is significant during panel buckling such as that exhibited in the current analysis, and inaccuracies in the modeling of the energy contained in such DOFs could seriously impact the results.

What remains somewhat puzzling about this conclusion, however, is that this discrepancy should have a stronger influence on the accuracy of the SHELL99 element even in the nonlinear buckling analysis, whereas this analysis proved to be reasonably accurate. It may be that in the step-by-step recalculation of the stiffness matrix in the nonlinear analysis, the SHELL99 formulation does a reasonably accurate estimation of the influence of high transverse strain that is occurring during buckling, but this conclusion is somewhat skeptical.

Therefore, it is not possible to provide further guidance regarding the circumstances or types of analyses in which the simplified formulation of the SHELL99 element would be appropriate. Therefore, the author recommends the exclusive use of higher-order elements. And although the linear buckling analysis with the higher order element was sufficiently accurate here, the nonlinear analysis still provided valuable insights into behavior that preceded failure at lower load factors. Therefore, the author also strongly recommends the use of nonlinear analysis as standard procedure in the design of wind turbine rotor blades.

4. References

[1] ANSYS, ver. 11.0, ANSYS, Inc. Canonsburg, Pennsylvania.

[2] *Guidelines for the Certification of Wind Turbines*, Edition 2003, Germanischer Lloyd, Hamburg, 01 November 2003.